Eccentricity distribution of wide binaries

A. Tokovinin[1]⋆ & O. Kiyaeva[2]†
[1] Cerro Tololo Inter-American Observatory, Casilla 603, La Serena, Chile
[2] Central Astronomical Observatory at Pulkovo, Pulkovskoe sh. 65/1, St. Petersburg 196140, Russia

Accepted XXX. Received YYY; in original form ZZZ

ABSTRACT

A sample of 477 solar-type binaries within 67 pc with projected separations larger than 50 AU is studied by a new statistical method. Speed and direction of the relative motion are determined from the short observed arcs or known orbits, and their joint distribution is compared to the numerical simulations. By inverting the observed distribution with the help of simulations, we find that average eccentricity of wide binaries is 0.59±0.02 and the eccentricity distribution can be modelled as $f(e) \approx 1.2e + 0.4$. However, wide binaries containing inner subsystems, i.e. triple or higher-order multiples, have significantly smaller eccentricities with the average $e = 0.52 \pm 0.05$ and the peak at $e \sim 0.5$. We find that the catalog of visual orbits is strongly biased against large eccentricities. A marginal evidence of eccentricity increasing with separation (or period) is found for this sample. Comparison with spectroscopic binaries proves the reality of the controversial period-eccentricity relation. The average eccentricity does increase with binary period, being 0.39 for periods from 10^2 to 10^3 days and 0.59 for the binaries studied here (10^5 to 10^6 days).

Key words: binaries: visual; methods: statistical

1 INTRODUCTION

A significant fraction of stars are born in binary and multiple systems. Statistics of their orbital parameters bear traces of formation history and help understanding its physics. Binary-star formation is an essential piece in such fundamental areas as stellar mass function, formation of planetary systems, and binary/stellar population synthesis.

Recent review of binary statistics by Duchêne & Kraus (2013) focuses on multiplicity fractions, periods, and mass ratios, mentioning the eccentricity distribution only briefly. Yet, eccentricity is an important diagnostic of binary formation. It is generally recognised that dynamical interactions in stellar systems produce binaries with "thermal" eccentricity distribution $f(e) = 2e$, predicted from general considerations by Ambartsumian (1937). On the other hand, binaries with mean eccentricities below 0.5 are formed in hydro-dynamical simulations as a result of dissipative interaction with surrounding gas which also decreases binary separations (Bate 2009). From this perspective, spectroscopic binaries should have lower eccentricities than wider visual binaries, and a general trend of increasing eccentricity with binary period is expected.

The relation between eccentricity and binary period, noted a long time ago, has been controversial ever since. While tidal circularisation at periods shorter than ∼10 days is well established, the situation at longer periods is not clear. Duquennoy & Mayor (1991) studied a small sample of nearby solar-type stars and found that at periods between 10 and 1000 days the mean eccentricity is 0.31, same as in nearby open clusters and halo. At longer periods, they found a "bell-shaped" eccentricity distribution and suggested that after correction of selection biases the data are compatible with the thermal distribution. In other words, they confirmed the period-eccentricity relation and implied that close and wide binaries were formed by different processes. However, Raghavan et al. (2010) have not found any dependence of eccentricity on period at $P > 10^3$ days in a similarly complete but larger sample; for 82 such binaries in their sample the mean eccentricity is 0.47. The eccentricity distribution appears uniform in the range [0-0.6] and falls at larger values (see their Fig. 15).

So far, studies of the eccentricity distribution were based on orbital elements, both spectroscopic and visual. Long-term radial-velocity monitoring can achieve a complete census of orbits in a given sample (e.g. Griffin 2012). Visual orbits are often constrained by the limited time coverage that extends only to ∼ 200 years in the best cases. While the discovery of visual binaries does not depend on the eccentricity, the orbit calculation does, introducing "computational selection" in the orbit catalogs (Finsen 1936). Both Duquennoy & Mayor (1991) and Raghavan et al. (2010) used visual orbit catalogs in their analysis of nearby samples.

⋆ E-mail: atokovinin@ctio.noao.edu
† E-mail: kiyaeva@list.ru

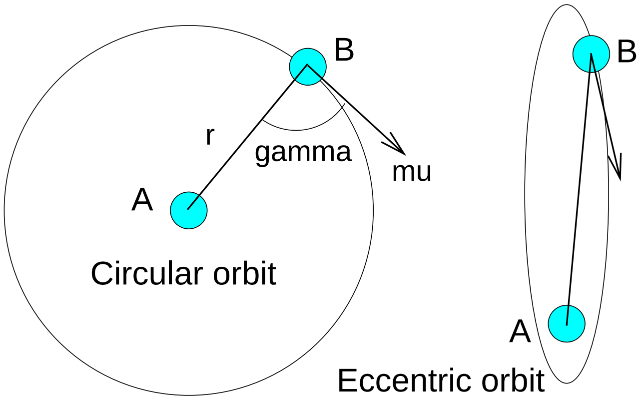

Figure 1. Scheme of the observed motion in a binary system. Left: circular orbit, right: eccentric orbit.

Based also on the catalogs of spectroscopic and visual orbits, Abt (2006) found that the average eccentricity of late-type stars increases with period and saturates at $\langle e \rangle = 0.52 \pm 0.02$ at $P > 10^5$ days. These findings, however, are likely biased by the computational selection inherent to the orbit catalogs.

In this paper we study the eccentricity distribution of wide visual binaries by a new method that does not rely on orbit calculation. It can access binaries with periods longer than 1000 years without computational selection bias. The idea is to use the direction and speed of the observed orbital motion. Only a short arc needs to be covered by the data. The statistics of the observed quasi-linear motion depend on the eccentricity distribution, which then can be reconstructed from the observational data without computing the orbits (Tokovinin 1998). This method has been used previously by Shatsky (2001); it will benefit from precise *Gaia* astrometry in the near future.

The method is explained in Section 2. Then in Section 3 we present the input data: a sample of solar-type visual binaries within 67 pc. Simulations are described in Section 4, the derived eccentricity distribution is given in Section 5, with the details of the restoration technique provided in the Appendix. The paper closes with the discussion of the results and summary in Section 6.

2 THE METHOD

Figure 1 explains the idea. When only a short segment of the orbit is observed, we can measure the speed of the relative orbital motion μ and the angle γ of the orbital motion relative to the vector joining the binary components. A circular orbit seen "face-on" will have $\gamma = \pm 90^\circ$, while for an eccentric orbit we expect a near-radial motion with $\gamma \sim 0^\circ$ or $\gamma \sim 180^\circ$. For binaries seen in projection on the sky at random orbital phases, statistical distributions of γ and μ still depend on the eccentricity. Throughout this paper we assume that binary orbits are oriented randomly (isotropically) relative to the line of sight.

Here we extend the method of Tokovinin (1998) by considering both parameters, γ and μ. Hereafter they are called linear motion parameters (LMPs). The joint distribution of (γ, μ) brings more information than just γ alone. Note however that while γ is a purely geometric parameter, the interpretation of μ requires knowledge of parallax and mass. Radial velocity difference between the components is yet another observable parameter that depends on the eccentricity; it is not exploited here.

There are several obstacles to our project. First, the LMPs of wide binaries can be distorted by motions in subsystems. For this reason we base our work on the FG-67 sample of solar-type stars within 67 pc (Tokovinin 2014a,b). This sample is large enough, while the subsystem census is reasonably good. Second, wide binaries move slowly and their motion may not be measurable from the available data. This limits the largest separations and longest periods amenable to such study. Third, we must avoid biases. For example, if we use only binaries with detectable motion, a bias on μ (and hence on eccentricity) could be introduced. However, removal of some systems from the statistical sample for lack of sufficient data is independent of their (unknown) eccentricity, hence it should not bias the result.

2.1 Main relations

Orbits and periods of wide binaries are not known. We use the projected separation $r = \rho/p$ (ρ is the angular separation, p is the parallax) as a proxy of the semi-major axis a. The third Kepler law allows a statistical estimate of the orbital period that we denote by P^*, to avoid confusion with the true period P. So,

$$r^3/(P^*)^2 = M \quad \text{or} \quad P^* = r^{3/2} M^{-1/2}, \tag{1}$$

where M is the mass sum in solar units and P^* is in years.

The characteristic orbital velocity is $2\pi r/P^*$ AU yr^{-1}. We multiply it by the parallax, converting to arcsec yr^{-1}, and obtain the characteristic speed of the relative orbital motion μ^* as

$$\mu^* = p(2\pi r)/P^* = 2\pi \rho^{-1/2} p^{3/2} M^{1/2}. \tag{2}$$

Strong dependence on the parallax p calls for selecting nearby stars. Also, close binaries move faster, but we are interested here in wide binaries! The sample is constructed by imposing some minimum value of $\mu^*_{\rm min}$. This is equivalent to an upper limit on separation $r_{\rm max}$ that depends on mass and distance,

$$r < r_{\rm max} = M\,(2\pi p/\mu^*_{\rm min})^2. \tag{3}$$

Simulations show that the ratio μ/μ^* is a random quantity depending on the orbital phase, projection, and eccentricity. Its median value is about 0.5. We compare the observed distributions of the normalised motion $\mu' = \mu/\mu^*$ and γ with the results of simulations. It can be easily proven that a bound binary system has $\mu' < \sqrt{2}$. This corresponds to the $B < 1$ criterion of Pearce et al. (2015). When the relative motion is faster than this, the double star is an optical pair (Kiyaeva et al. 2008). Considering measurement errors, we adopt a slightly relaxed criterion $\mu' < 1.5$ for physical pairs.

3 OBSERVATIONAL DATA

3.1 The sample

Our main sample consists of solar-type binary systems within 67 pc from (Tokovinin 2014a, hereafter FG-67) with

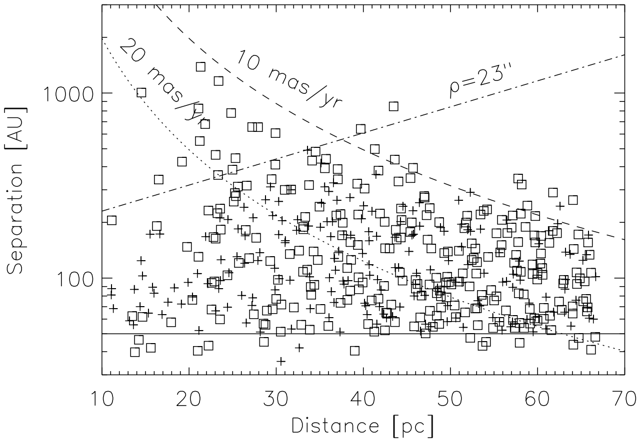

Figure 2. Projected separations of wide binaries studied here (squares – main sample, crosses – extended sample). The dashed and dotted lines depict upper limits on projected separation for $\mu^*_{\rm min} = 10\,{\rm mas\,yr}^{-1}$ and $\mu^*_{\rm min} = 20\,{\rm mas\,yr}^{-1}$, respectively, adopting $M = 2\mathcal{M}_\odot$. Angular separation of $23''$ is indicated by the dash-dot line.

projected separations $r > 50$ AU. The initial selection of 886 physical pairs was further filtered by the criterion $\mu^* > 10\,{\rm mas\,yr}^{-1}$, leaving 344 objects. This restriction is dictated by the accuracy of LMP determination from the available data. The masses of both components (including known subsystems) needed for the calculation of μ^* are taken from the FG-67 compilation, the parallaxes are from (van Leeuwen 2007).

The main sample was complemented by additional binaries from the *Hipparcos* catalog with parallax larger than 15 mas and projected separation larger than 50 AU (minimum separation of $0\farcs75$ at a distance of 67 pc). The *Hipparcos* catalog lists only binaries with separations up to $23''$, restricting the maximum projected separations. Stars that already belong to the main sample were excluded from the extension. For stars with masses less than $\sim 0.8\,\mathcal{M}_\odot$, *Hipparcos* is not complete to 67 pc, so the extended sample is also not complete, while still being volume-limited.

Visual magnitudes of the components of the extended sample were taken from the Washington Double Star Catalog (WDS, Mason et al. 2001). Masses were estimated from absolute magnitudes in the V band using standard relations for main sequence, as in (Tokovinin 2014a). Objects with primary mass larger than $2\,\mathcal{M}_\odot$ were removed (22 total), as their masses are not determined well by the standard relations. Then the characteristic speed μ^* was computed and only binaries with $\mu^* > 10\,{\rm mas\ yr}^{-1}$ were kept. This left 231 binaries in the extended sample. The combined sample thus contains 575 entries. Figure 2 shows projected separations versus distance and the selection limits of our samples. As explained below, only 85% of binaries are included in the statistical analysis, the rest having insufficient data for LMP determination.

The census of subsystems in the FG-67 paper is as complete as possible, with well-known detection limits (∼80% complete for subsystems in the primary components and ∼50% for the secondary subsystems). In the extended sample, however, the detection of subsystems is less complete. It was cross-checked with the latest (2010) version of the Multiple Star Catalog (Tokovinin 1997), revealing only 27 pairs with subsystems out of 231. The combined list contains 113 multiples (88 subsystems in the primary, 40 in the secondary, 15 in both). Overall, 20% of wide binaries in the combined sample and 25% in the main sample contain known inner subsystems. In a population simulated according to the prescription of (Tokovinin 2014b), 48% of binaries with periods from 10^5 to 10^6 days have subsystems. Orbital periods of most subsystems are shorter than the time span of the data, so they should not distort the LMPs. There are a few notable exceptions, however, such as HIP 17129. Some binaries have even wider components, but this circumstance is neglected in the present work.

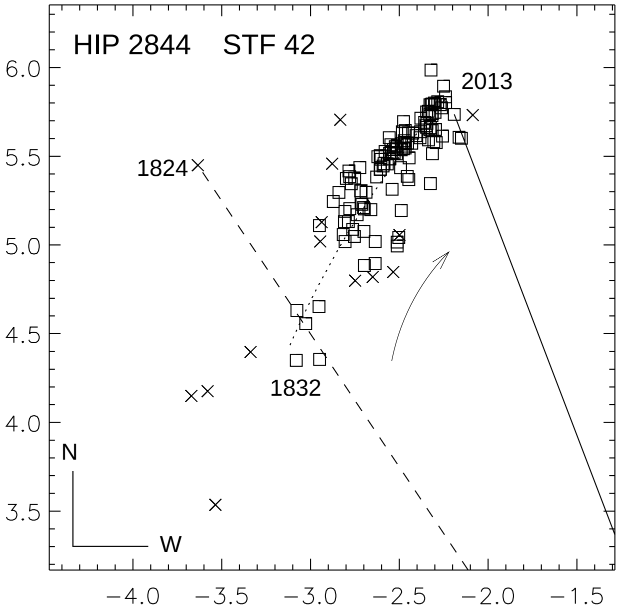

Figure 3. Observed motion of HIP 2844 (00360+2959, STF 42 AB). Scale in arcseconds, North up, East left. Squares mark used measurements (first in 1832), crosses – rejected ones. The dashed and full lines connect the primary component located at coordinate origin with the first and last positions of the companion. The dotted line is the LMP trajectory.

3.2 Determination of linear motion

Measurements of the relative positions of selected binary stars (time, position angle, separation) were obtained from the WDS on our request. Apart from the *Hipparcos* number, each binary is identified by its WDS code based on J2000 coordinates and by the discoverer code; the latter discriminates between several catalog entries with the same WDS code, e.g. resolved subsystems.

The motion in position angle θ and separation ρ was approximated by linear functions of time:

$$\theta(t) \approx \theta_0 + \dot{\theta}(t - t_0) \quad (4)$$

$$\rho(t) \approx \rho_0 + \dot{\rho}(t - t_0). \quad (5)$$

The reference time moment t_0 is the average time of observations, as in such case the slope and mean value are not correlated. The four LMPs are $(\theta_0, \dot{\theta}, \rho_0, \dot{\rho})$. Motion of binaries is better represented by linear models in polar coordinates than in rectangular coordinates X, Y (consider a circular face-on orbit for example).

The LMPs are computed from the measured speed of relative angular and radial motions $\mu_t = \rho_0 \dot\theta$ and $\mu_r = \dot\rho$, so that $\mu = \sqrt{\mu_t^2 + \mu_r^2}$ and $\gamma = \mathrm{atan}(\mu_t, \mu_r)$. The errors of the fitted LMPs are computed in the standard way. We assume that all LPMs are statistically independent and determine the errors of μ and γ accordingly as

$$\sigma_\mu^2 = \mu^{-2} \, [(\dot\rho \sigma_{\dot\rho})^2 + (\rho_0^2 \dot\theta \sigma_{\dot\theta})^2 + (\rho_0 \dot\theta^2 \sigma_{\rho_0})^2], \quad (6)$$

$$\sigma_\gamma^2 = \mu^{-4} \, [(\dot\rho \sigma_{\dot\rho})^2 + (\rho_0 \sigma_{\dot\rho} \sigma_{\dot\theta})^2 + (\dot\rho \dot\theta \sigma_{\rho_0})^2]. \quad (7)$$

Figure 3 illustrates typical data. The dashed and solid lines connect the first and last positions, respectively, with the primary component located at coordinate origin outside the plot. The dotted arc is a linear motion in polar coordinates. Points deviating by more than 3σ from the fit in either ρ or θ were rejected iteratively (they are plotted as crosses). All remaining measurements (squares) are considered with equal weights.

Observations of some binaries cover a substantial arc. In such situations, we separated the data into segments with angular motion of no more than 20°. We also require each data segment to contain at least three points and to cover the time interval of no less than two years. The LMPs computed over the last data segment (typically the most accurate) are taken as the final values.

The quality and quantity of available data is very diverse; in some cases the measurements have a strong scatter and the LMPs are determined with large errors. In a few cases, one or two strongly deviant measurements were deleted manually. For some binaries, the data are not sufficient. This happens for recently discovered pairs with a short time coverage and for binaries with only a few measurements of low accuracy. Several binaries with $\rho > 10''$ also fall in this category, as measurement errors usually increase with separation. These pairs were excluded from the statistical analysis. We also excluded binaries with errors of γ exceeding 15°. All binaries are physical, as their relative motion is slow enough ($\mu' < 1.5$, see Section 2.1).

For some binaries in our sample we found visual orbits in the Sixth Catalog of Orbits of Visual Binary Stars, VB6 (Hartkopf & Mason 2013). Considering only 150 orbits with periods shorter that 2500 yr, we computed the LMPs for the same moments t_0 from the orbital elements and used those. Comparison of "orbital" and directly derived LMPs shows their excellent agreement, which is natural because both are based on the same observations. In the extended sample, we did not request the observations of orbital pairs from the WDS and simply used their orbits to compute the LMPs for $t_0 = 1991.25$.

For pairs with known visual orbits, the FG-67 database lists semi-major axis instead of separation. We removed from the sample orbital binaries with projected separations less than 40 AU; they were included by error because their semi-major axis exceeds 50 AU. However, 13 orbital binaries with separations between 40 and 50 AU were retained. On the other hand, some orbital pairs with semi-major axis less than 50 AU but projected separations exceeding 50 AU were rejected initially, but later recovered in the extended sample and moved back to the main sample.

Table 1. Median parameters of the samples

Sample	N	p mas	M_1 $\mathcal{M}_\odot$	ρ $''$	r AU	μ mas yr^{-1}	μ^*
Main	344	22.9	1.15	2.93	130.3	11.2	17.6
Extended	231	24.8	0.87	3.27	110.2	12.0	18.5
Combined	575	23.8	1.09	3.08	122.0	11.5	18.1
Simulated	...	20.5	...	2.59	122.2	9.3	16.6

3.3 Data overview and tables

The combined sample contains 575 wide binaries, but only 477 pairs with good data are left for statistical analysis. The median parameters of the main, extended, and combined samples are listed in Table 1. As expected, the extended sample has a smaller mass of primary components and is on average located at closer distance compared to the main sample. The last line of the Table characterises the simulated sample (Section 4.2).

Orbital periods P^* estimated from projected separations are mostly comprised between 10^5 and 10^6 days, i.e. on the right-hand side of the maximum in the period distribution at 10^5 days (Raghavan et al. 2010; Tokovinin 2014b). As we deal here with resolved visual binaries, their mass ratios are mostly above 0.5 (median 0.75).

The median errors of μ and γ are 0.5 mas yr^{-1} and 2.6°, respectively. The actual distribution of those errors closely matches negative-exponential, $f(\sigma_\mu) \propto \exp(-\sigma_\mu/0.8)$ and $f(\sigma_\gamma) \propto \exp(-\sigma_\gamma/3.8)$. Note that the 5% error on μ and the 3° error on γ match each other.

The Referee pointed out that rejection of binaries with $\sigma_\gamma > 15°$ might bias the statistics, as binaries on eccentric orbits near apastron move slowly and might be preferentially excluded from the sample by this criterion. The above exponential formula predicts that only 2 per cent of binaries would have σ_γ exceeding 15°, while in reality there are 57 such pairs (five times more), suggesting that most rejections are simply worse-than-average data. A small fraction of the rejected binaries can indeed be eccentric pairs near apastron, but the bias caused by their rejection should be correspondingly small. Unfortunately, the diversity of the data quality does not allow an easy evaluation of such bias by simulation. The median separation of the 57 pairs rejected by the $\sigma_\gamma > 15°$ criterion is $4\overset{''}{.}7$, wider than in the complete sample, while their median relative motion is slower, 7 mas yr^{-1} (median $\mu' = 0.36$).

The median characteristics of 150 binaries with known orbits belonging to the combined sample are: period 528 yr, semi-major axis $2\overset{''}{.}22$, mean eccentricity 0.53.

Table 2, available in full electronically, lists both samples ordered by the Hipparcos number in Column (1). Column (2) contains the WDS code, Column (3) the discoverer code. The following columns list (4): parallax in mas, (5): projected separation in AU, (6) and (7): masses of the primary and secondary components in solar units, (8): characteristic motion μ^* in mas yr^{-1}. Then in Column (9) a 1-letter code describing the type of motion is given: L for a short arc (linear), C for a large and curved arc or a substantial (at least factor 1.5) change in separation (this classification is subjective), and O for binaries with known orbits. Letter M is added to the type for binaries containing known inner

Table 2. Wide binaries within 67 pc (fragment)

HIP	WDS	Discovever code	p mas	r AU	M_1 $\mathcal{M}_\odot$	M_2 $\mathcal{M}_\odot$	μ^* mas yr^{-1}	Type	Tag
50	00006−5306	HJ 5437	16.8	105.1	1.55	0.87	16.1	C	M
96	00012+1357	WNO 12	28.5	418.2	0.68	0.64	10.1	L	E
110	00014+3937	HLD 60	20.1	58.1	0.91	0.84	22.0	O	E
169	00021−6817	I 699 AB	65.2	64.6	0.61	0.53	54.3	O	E
223	00028+0208	BU 281 AB	23.5	65.0	1.17	0.84	25.9	L	M
473	00057+4549	STT 547 AB	88.4	68.4	0.61	0.60	74.1	O	E
495	00059+1805	STF 3060 AB	26.9	130.1	0.88	0.79	19.2	L	M
522	00063−4905	HDO 180	38.9	120.6	2.25	0.54	37.2	LM	M
1292	00162−7951	CVN 14	57.2	67.6	0.95	0.45	51.7	L	m

Table 3. Linear motion parameters of binaries (fragment)

HIP	Type	t_0, Δt yr	θ_0 deg	$\dot\theta$ deg yr^{-1}	ρ_0 $''$	$\dot\rho$ $''$yr^{-1}	μ mas yr^{-1}	γ deg	μ', rms $^\circ/''$
50	C	1981.6	321.282	0.372	1.769	−0.0078	13.9	124.2	0.87
		52.9	0.647	0.034	0.029	0.0016	1.2	5.3	2.5/0.11
96	L	1980.8	203.971	0.003	11.897	−0.0052	5.2	174.0	0.52
		108.1	0.080	0.003	0.083	0.0029	3.0	7.2	0.4/0.38
110	O	1991.2	176.367	−0.430	1.171	0.0076	11.6	−49.2	0.53
169	O	1991.2	125.191	0.213	4.212	0.0068	17.1	66.6	0.31
223	L	1984.0	170.567	−0.349	1.526	0.0014	9.4	−81.7	0.36
		57.0	0.198	0.010	0.015	0.0008	0.8	4.7	1.0/0.07
473	O	1991.2	178.737	0.417	6.050	0.0044	44.3	84.3	0.60
495	L	1949.3	125.756	0.132	3.504	−0.0019	8.3	103.4	0.43
		155.3	0.062	0.002	0.008	0.0002	0.1	1.5	0.7/0.10

subsystems. The last Column (10) has the following flags: M for the main sample with known LMP, E for the extended sample with known LMP, m and e — binaries from the main and extended samples, respectively, excluded from the statistical analysis for lack of sufficient data.

Table 3 lists the LMPs of binaries used in this work (flags M and E). The Columns (1) and (2) repeat the *Hipparcos* number and type of data from Table 2. Column (3) contains the mean epoch t_0 in Besselian years. The following Columns (4) through (7) list the LMPs: θ_0 (degrees), $\dot\theta$ (degrees yr^{-1}), ρ_0 (arcsec), $\dot\rho$ (arcsec yr^{-1}). The LMPs are used to compute the total motion μ given in Column (8) in mas yr^{-1} and the angle γ in Column (9), in degrees and with proper sign. The last Column (10) gives the normalised motion $\mu' = \mu/\mu^*$. When the LMPs were determined here, the following line of Table 3 gives their errors in the same units. Column (3) of the second line then contains the time span of the data in years and Column (10) contains the rms scatter from the linear elements in θ and ρ, in degrees and arcseconds respectively. When the LMPs are calculated from the orbits (type O), no errors are given.

The following statistical analysis uses only two parameters μ' and γ. The angles are transformed into the interval (0,90°), i.e. we set $\gamma \rightarrow |\gamma|$ for $-90^\circ < \gamma < 90^\circ$ and $\gamma \rightarrow 180^\circ - |\gamma|$ otherwise. The characteristic speed μ^* is computed with *Hipparcos* parallaxes and estimated masses. If the masses are biased (e.g. by not accounting for additional unknown components), this bias affects μ^* and μ'. Comparison with simulations shows a good agreement in the median μ' values, so the bias, if any, should be small.

4 SIMULATIONS

4.1 Simple binaries

Our simulation code generates a large number N of binaries with a given eccentricity distribution. Orbital elements that do not influence the shape of the orbit (period $P = 1$ and semi-major axis $a = 1$) take fixed dimensionless values. The longitude of periastron ω is uniformly distributed in the interval $[0^\circ, 360^\circ]$, the inclinations i are in the $[0^\circ, 90^\circ]$ interval with a uniform distribution of $\cos i$. The binary position is calculated for some random moment of time and for the moment $0.005P$ later. The tangential and radial components of the relative motion are computed from the displacement over $0.005P$, giving the total speed μ (in the same dimensionless units) and its direction γ relative to the radius-vector. As we simulate only systems with direct motion ($i \leq 90^\circ$), all γ are non-negative. They are "folded" into the $[0^\circ, 90^\circ]$ interval. The normalised motion $\mu' = \mu\rho^{1/2}/(2\pi)$, where ρ is the "observed" separation of each binary.

Figure 4 illustrates the distribution of the parameters (μ', γ) for a relatively small number $N = 1000$ of simulated binaries. Near-circular orbits have a strong concentration to $(\mu', \gamma) \sim (1, 90^\circ)$, despite projection. Owing to random projection of the orbits, some circular binaries have $\gamma < 90^\circ$ and move at a slower normalized speed (remember that μ' contains the factor $\rho^{1/2}$, meaning that orbital motion appears slower than expected when the binary is seen at close separation). There is a positive correlation between μ' and γ. In contrast, γ decreases and the correlation becomes negative

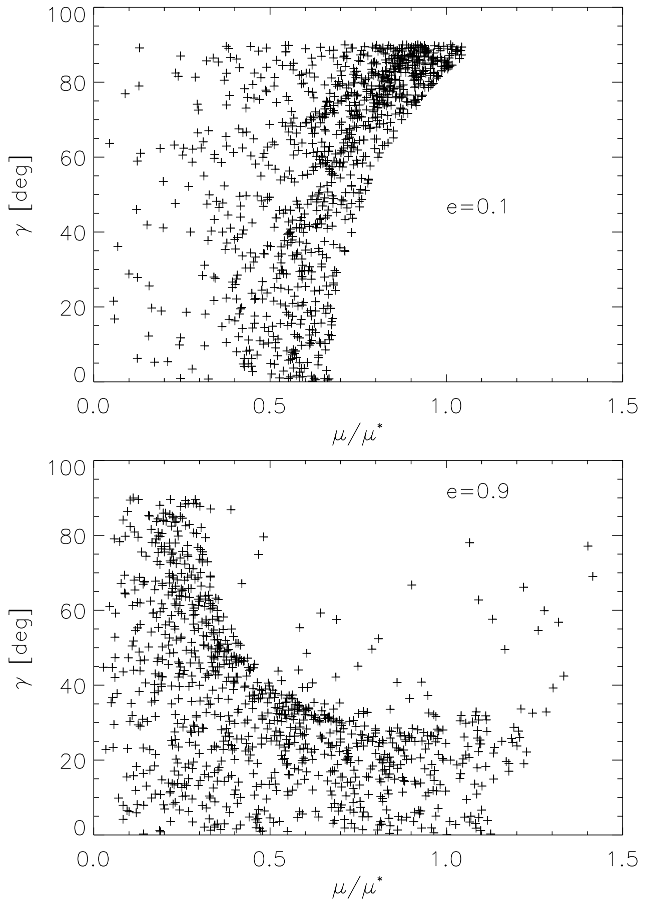

Figure 4. Relation between the normalised relative motion $\mu' = \mu/\mu^*$ and angle γ for simulated binaries with $e = 0.1$ (top) and $e = 0.9$ (bottom). Each plot contains $N = 1000$ points.

for eccentric orbits. Figure 5 shows the dependence of the median angle γ_m on eccentricity.

We demonstrate by simulation that the thermal eccentricity distribution $f(e) = 2e$ corresponds to the strictly uniform distribution of γ which is uncorrelated with μ'. Also, for circular orbits the strict inequality $\mu' \leq 1$ holds, while $\mu' < \sqrt{2}$ for all bound binaries. In the real binaries, $\mu' > 1.5$ occurs due to the LMP errors, when the binaries are optical (chance projections), or when they contain subsystems. We compute statistics only for $0 < \mu' < 1.5$, excluding a few cases with larger μ'.

4.2 Sampling biases

We studied by simulation the influence of our sampling criteria and measurement errors on the (μ', γ) statistics. To do so, we simulated a realistic population of binaries distributed uniformly in a volume of 67-pc radius. The periods are drawn from the log-normal distribution of Raghavan et al. (2010) restricted to the range from 100 to 10^5 yr. The mass sum of $2\,\mathcal{M}_\odot$ is assumed. Binaries are simulated as before, the parameters μ and γ are distorted by observational errors that match the real ones. The statistics are calculated for the whole population (which is equivalent to the results for simple binaries) and for the sub-sample with projected separation above 50 AU and $\mu^* > 10\,\mathrm{mas\,yr}^{-1}$. These criteria reject very close and very wide binaries, respectively (Figure 2). About 45% of the simulated population passes the selection criteria. In the following we use the results of these more realistic sample simulations.

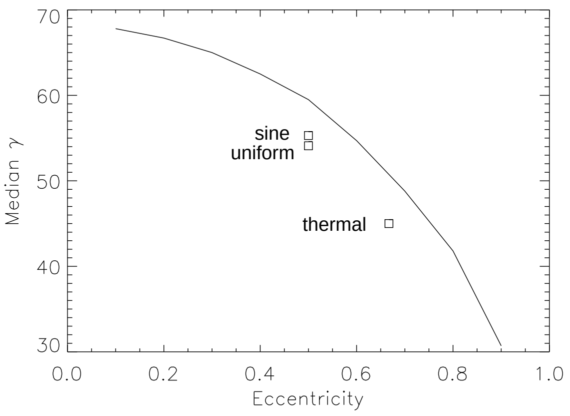

Figure 5. Results of simulations for simple binaries: dependence of the median γ on the eccentricity. The curve is for binaries of fixed eccentricity, while squares depict simulated samples with thermal, uniform, and sine eccentricity distributions, where their mean eccentricity is plotted.

Table 4. Results of simulations and observed parameters

Eccentricity	μ'_m	γ_m	C	μ'_m	γ_m	C
	Simple binaries			Sample simulation		
$e = 0$	0.677	68.3	0.61	0.678	67.4	0.26
$e = 0.3$	0.660	65.7	0.43	0.674	65.9	0.19
$e = 0.6$	0.577	53.1	0.03	0.590	55.0	0.02
$e = 0.9$	0.437	31.2	−0.44	0.432	30.5	−0.41
Uniform	0.606	54.1	0.18	0.608	53.5	0.08
Sine	0.609	55.3	0.15	0.610	56.0	0.07
Thermal	0.546	45.0	0.00	0.549	44.7	0.00
Combined (477)	...	...	...	0.58	48.6	0.11
Main (282)	...	...	...	0.57	47.4	0.07
Multiples (92)	...	...	...	0.65	56.6	0.25
Binaries (385)	...	...	...	0.57	47.5	0.08

After selection, the simulated sample is a close match to the real one (see the last line in Table 1). The median parallax is a little less than in the main sample, reflecting its ~10% incompleteness (Tokovinin 2014a). Median parameters of the simulated sample do not depend on the adopted eccentricity distribution.

We found that the sample selection does not bias the median values of μ' and γ in any significant way. However, their correlation can be reduced in absolute value by as much as a factor of ~2.

Table 4 quantifies the simulation results using $N = 10\,000$ simulated binaries for each case. It lists the *median* values of the main parameters μ'_m and γ_m and their correlation coefficient C. As the eccentricity increases, the normalised motion becomes slower, γ_m decreases, and the correlation becomes negative. The right-hand part of the Table reports results of sample simulations that account for biases. The sine eccentricity distribution is $f(e) = \pi/2 \sin(\pi e)$.

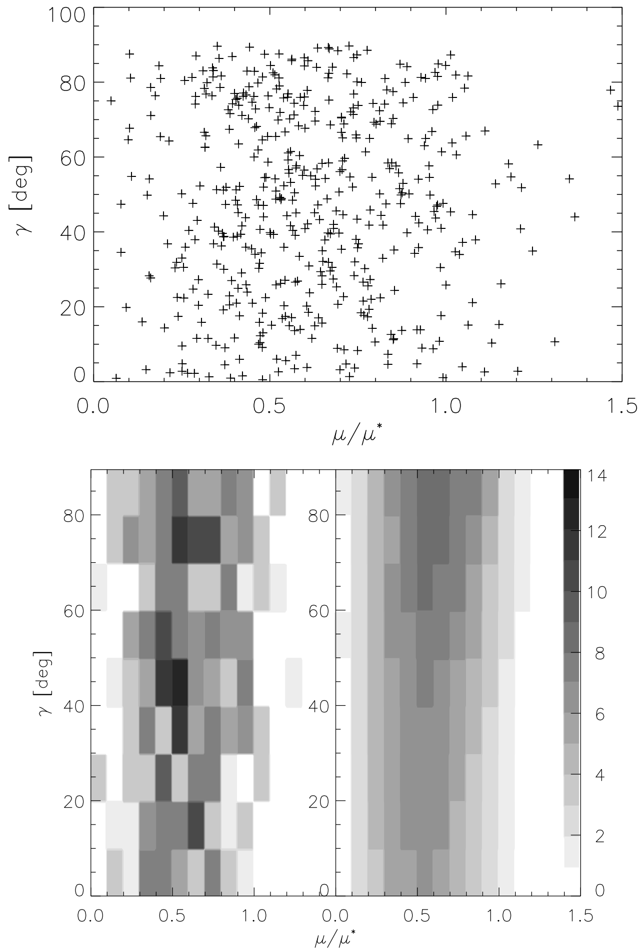

Figure 6. Top: relation between μ' and γ for 475 binaries in the combined sample. Bottom: the grayscale histogram of the data in 15×9 bins on the left is compared to the fitted model on the right. The scale bar on the right shows data counts in the histogram.

5 RESULTS

Figure 6 (top) shows the observed values of μ' and γ. The median parameters and correlation are given in the last lines of Table 4 for direct comparison with simulations.

The 5-bin eccentricity distribution was determined by the regularised least-squares method described in the Appendix. Briefly, the two-dimensional histogram of μ', γ is approximated by a linear combination of five histograms produced by simulations, where each simulated histogram corresponds to the eccentricity comprised in one bin. The result is a set of five numbers f_k representing fractional content of each bin, with $\sum_k f_k = 1$. The lower part of Figure 6 illustrates how the real two-dimensional histogram is matched by its model.

The errors of f_k are estimated by the bootstrap technique. We generated 50 artificial data sets by selecting randomly the same number of binaries from the original data (i.e. some data are skipped, some appear several times). The distribution was determined for each set and averaged, while its rms scatter estimates the errors. The average eccentricity is determined more accurately than the distribution itself. Errors delivered by bootstrap were confirmed by analysis of simulated samples, thus verifying the method.

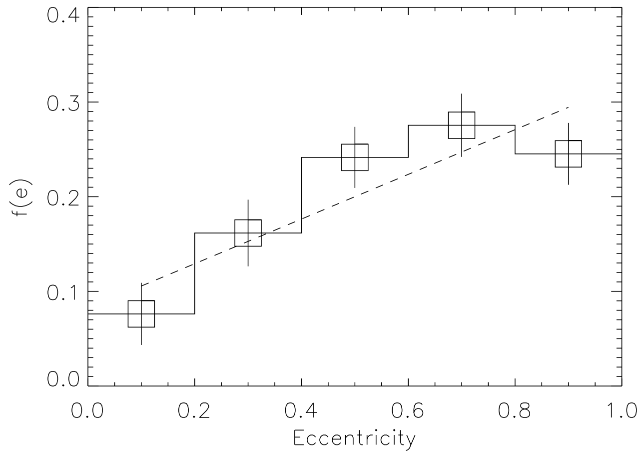

Figure 7. Eccentricity distribution of wide binaries and its errors determined by bootstrap for the combined sample. The dashed line is a linear model $f(e) = 1.2e + 0.4$.

Table 5 lists the resulting 5-bin distributions and their errors for the main and combined samples and various sub-samples. Two binaries with $\mu' > 1.5$ are not considered, reducing the combined sample size from 477 to 475. The derived eccentricity distribution is plotted in Figure 7. A linear model $f(e) = 2 f_{\rm lin} e + 1 - f_{\rm lin}$ (sum of thermal and uniform distributions) was also fitted to the (μ', γ) data; we give $f_{\rm lin}$ in the right column of Table 5.

To study the dependence of eccentricity on separation, we divided the combined sample in two approximately equal parts with projected separations less or larger than 100 AU. The average eccentricities are 0.56 ± 0.03 and 0.62 ± 0.03, respectively, and the eccentricity distribution becomes closer to a thermal one with increasing separation. The median mass ratios in these two groups are comparable, 0.77 and 0.72.

There is evidence of different eccentricity distributions in pure binaries and binaries containing subsystems. This matches the difference in the median angles γ between these sub-samples (see Table 4). The eccentricity distribution reconstructed for 92 multiples in the combined sample has a strong peak in the third bin $e =$[0.4-0.6], $f_3 = 0.40$. The average eccentricity of multiples is 0.52 ± 0.05, significantly less than for binaries in general. Remember that many "binaries" contain undetected subsystems, so the actual difference may be even larger than found here.

6 DISCUSSION

The eccentricity distribution of wide binaries is "softer" than the thermal one, containing more orbits with $e < 0.2$ and less orbits with $e > 0.8$. To our knowledge, this is the first observational determination of $f(e)$ for wide binaries. The *ad hoc* initial eccentricity distribution adopted in N-body simulations (e.g. Marks et al. 2011, their Figure 2) is closer to $f(e) = 2e$ than the real one. These authors found that the eccentricity distribution is not affected by dynamical evolution of binaries in a cluster. Some binaries are simply

Table 5. Derived eccentricity distributions

Sample (N)	f_1	f_2	f_3	f_4	f_5	$\langle e \rangle$	$f_{\rm lin}$
Combined	0.08	0.16	0.24	0.28	0.25	0.59	0.59
(475)	±0.03	0.04	0.03	0.03	0.03	0.02	
Main	0.04	0.19	0.24	0.23	0.29	0.62	0.73
(280)	±0.03	0.04	0.05	0.05	0.05	0.02	
Extended	0.14	0.14	0.20	0.33	0.19	0.56	0.39
(195)	±0.06	0.06	0.05	0.06	0.06	0.03	
Multiples	0.12	0.17	0.40	0.15	0.17	0.52	0.04
(92)	±0.08	0.08	0.10	0.08	0.08	0.05	
$r < 100$AU	0.13	0.15	0.21	0.31	0.19	0.56	0.37
(218)	±0.05	0.05	0.06	0.07	0.05	0.03	
$r > 100$AU	0.03	0.18	0.26	0.23	0.30	0.62	0.75
(256)	±0.04	0.05	0.05	0.05	0.04	0.03	

disrupted, while the remaining binaries are unchanged. This means that $f(e)$ for field binaries reflects their formation mechanism.

Appreciable difference in the eccentricities of wide binaries with and without subsystems is a new result, confirming the work of Shatsky (2001). In the hindsight, such a difference is expected because very eccentric outer orbits are not allowed by dynamical stability of multiple systems. Using the statistical multiplicity model proposed by Tokovinin (2014b), we generated a synthetic population of triples with outer periods from 250 to 8000 years containing subsystems with period ratios $P_{\rm OUT}/P_{\rm IN} > 4.7$ in one of their components. Assuming that the outer orbits have thermal eccentricity distribution, we removed triples that do not conform to the dynamical stability criterion by Mardling & Aarseth (2002),

$$P_{\rm OUT}(1-e)^{1.8}(1+e)^{-0.6} > 4.7 P_{\rm IN}, \qquad (8)$$

and found that the remaining outer systems have average eccentricity of ∼0.55, in qualitative agreement with the actual multiple systems. We provide this crude estimate only as an illustration because its underlying assumptions are unrealistic. It is more likely that formation mechanisms of multiple systems favour moderate eccentricities in outer orbits.

It is instructive to compare our results with the distribution of eccentricities in known visual orbits. We selected orbits of grade 3 or better from the VB6 catalog (Hartkopf & Mason 2013) and found a bell-shaped distribution of e declining towards large eccentricities (Figure 8). There is a tendency of smaller eccentricity at shorter orbital periods. For 581 orbits with $P < 100$ yr (median period 27 yr) we find $\langle e \rangle = 0.45$, while for 243 orbits with $P > 100$ yr (median period 158 yr) $\langle e \rangle = 0.51$. Orbits determined from a short observed arc often have a strong positive correlation between period and eccentricity, so it is not clear to what extent the VB6 trend of eccentricity increasing with period is genuine.

Comparing the eccentricity distribution of $P > 100$ yr orbits in VB6 with the distribution derived here, we note their similarity up to $e \sim 0.8$ and the strong deficit of larger eccentricities in VB6. This is most certainly related to the computational selection discussed by Finsen (1936). There are many binaries in our sample with nearly radial motion and substantial time coverage, but without computed orbits. The mean eccentricity of visual binaries derived by Abt (2006), Raghavan et al. (2010) and others should be biased to lower values by this effect.

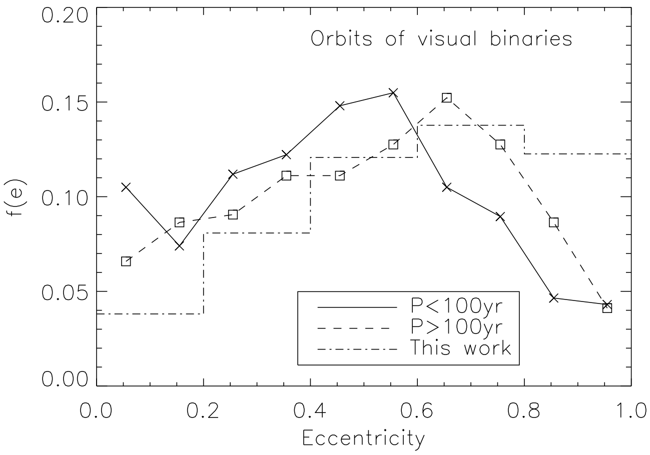

Figure 8. Distribution of eccentricity in the VB6 for orbits of grade 3 or better. Full line: 581 orbits with $P < 100$ yr, dashed line: 243 orbits with $P > 100$ yr. Average eccentricities are 0.45 and 0.51, respectively. The dash-dot line is our result for the combined sample normalised for bin size of 0.1.

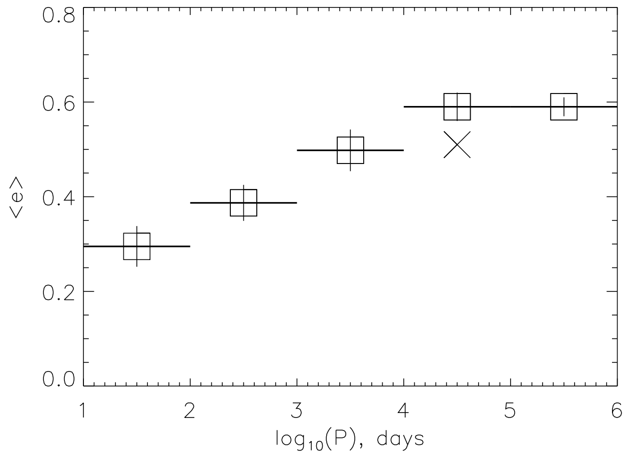

Figure 9. Period-eccentricity relation. Horizontal lines depict period ranges and average eccentricity in these ranges according to Udry et al. (1998), Griffin (2012), Abt (2006) (cross, underestimated), and this work (the last two period intervals). The errors are shown by vertical lines.

We note that VB6 contains a heterogeneous sample of binaries dominated by nearby low-mass stars. The errors and biases of orbital eccentricities in VB6 are unknown. The method used here avoids uncertainties and biases associated with orbit calculation.

The computational selection is less of a problem for spectroscopic binaries. Very long time coverage of binaries in the Hyades by Griffin (2012) is particularly useful in this respect. His Table 1 contains 29 orbits with $P > 10^3$ days (and mostly $P < 10^4$ days) with a nearly uniform eccentricity distribution and a mean eccentricity of 0.498±0.044. On the other hand, the average eccentricity of solar-type binaries with periods from 10 to 10^3 days in the field and in open clusters is less, 0.31 (Duquennoy & Mayor 1991). Using more extensive data of Figure 3 from Udry et al. (1998), we compute $\langle e \rangle = 0.295 \pm 0.043$ for $10 < P < 100$ days and $\langle e \rangle = 0.387 \pm 0.038$ for $100 < P < 1000$ days for a total of 198 orbits in these period intervals.

To probe the eccentricity distribution at intermediate periods, we selected 210 visual binaries with projected separations from 10 to 50 AU from the main 67-pc sample, covering approximately the period range $10^4 < P < 10^5$ days, and repeated the statistical analysis done for wider binaries. In this group, 155 binaries have known orbits. To avoid confusion, we do not provide more details of this supplementary study and only use the derived average eccentricity $\langle e \rangle = 0.59 \pm 0.03$ in the discussion.

The dependence of average eccentricity on period is presented graphically in Figure 9. At orbital periods longer than 10^2 days the eccentricity can be as high as 0.9, meaning that tidal circularisation is not important. Still, the mean eccentricity continues to increase with period.

Main results of this study can be summarised as follows:

(i) Eccentricities of wide (median separation ∼120 AU) nearby (within 67 pc) low-mass binaries in the field are distributed as $f(e) \approx 1.2e + 0.4$, with $\langle e \rangle = 0.59 \pm 0.02$.

(ii) We found marginal evidence of average eccentricity increasing with binary separation. Comparison with spectroscopic binaries in the field puts this increase beyond doubt, confirming the period-eccentricity trend.

(iii) Visual binaries with high eccentricities are strongly under-represented in the current orbit catalogs, biasing statistics derived from the catalogs.

(iv) Eccentricities of wide binaries containing subsystems are significantly less than for the rest of the sample, $\langle e \rangle = 0.52 \pm 0.05$. This can be explained, at least partially, by dynamical stability of multiple systems that does not allow very eccentric outer orbits.

ACKNOWLEDGEMENTS

This work used binary-star measurements collected in the Washington Double Star Catalog maintained at USNO. We thank W. Hartkopf for extracting the measurements on our request and stress the usefulness of keeping and updating the WDS database. Thoughtful comments by the anonymous Referee are much appreciated. We used the SIMBAD service operated by Centre des Données Stellaires (Strasbourg, France) and bibliographic references from the Astrophysics Data System maintained by SAO/NASA.

REFERENCES

Abt, H. A. 2006, ApJ, 651, 1152
Ambartsumian, V. 1937, Astr. Zh., 14, 207
Bate, M. R. 2009, MNRAS, 393, 590
Duchêne, G. & Kraus, A. 2013, ARAA, 51, 269
Duquennoy, A. & Mayor, M. 1991, A&A, 248, 485
Finsen, W. S. 1936, MNRAS, 96, 862
Griffin, R. F. 2012, JAA, 33, 29
Hartkopf, W. I. & Mason, B. D. 2015, Sixth Catalog of Orbits of Visual Binary Stars. USNO http://www.usno.navy.mil/USNO/astrometry/optical-IR-prod/wds/orb6.html (VB6)

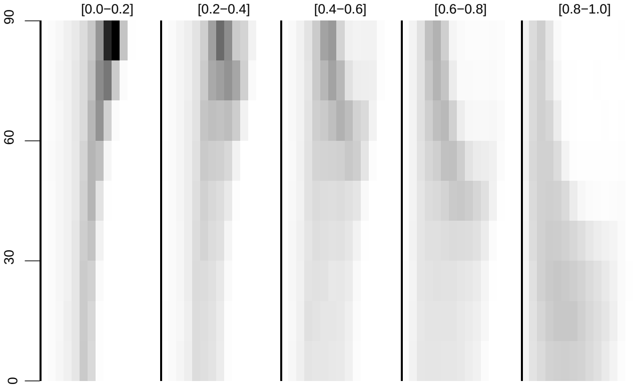

Figure A1. Grayscale representation of the (μ', γ) probability distributions. Left to right: eccentricity intervals [0-0.2], [0.2-0.4], etc. The horizontal range of each panel in μ' is from 0 to 1.5, the vertical range in γ is from 0 to 90°. The intensity scale is equal for all panels.

Kiyaeva, O. V., Kiselev, A. A., & Izmailov, I. S. 2008, AstL, 34, 405
Mardling, R. A. & Aarseth, S. E. 2002, MNRAS, 321, 398
Marks, M., Kroupa, P., & Oh, S. 2011, MNRAS, 417, 1684
Mason, B. D., Wycoff, G. L., Hartkopf, W. I., Douglass, G. G. & Worley, C. E. 2001, AJ, 122, 3466 (WDS) http://www.usno.navy.mil/USNO/astrometry/optical-IR-prod/wds/wds.html
Pearce, T. D., Wyatt, M. C., & Kennedy, G. M. 2015, MNRAS, 448, 3679
Raghavan, D., McAlister, H. A., Henry, T. J. et al. 2010, ApJS, 190, 1
Shatsky, N. 2001, A&A, 380, 238
Tokovinin, A. 1998, AstL, 24, 178
Tokovinin, A. 1997, A&AS 124, 75 (MSC) http://www.ctio.noao.edu/~atokovin/stars/index.php
Tokovinin, A. 2014a, AJ, 147, 86 (FG-67)
Tokovinin, A. 2014b, AJ, 147, 87
Udry, S., Mayor, M., Latham, D. W. et al. 1998, in: The Tenth Cambridge Workshop on Cool Stars, Stellar Systems and the Sun, Eds. R. A. Donahue & J. A. Bookbinder. ASP Conf. Ser., 154, 2148
van Leeuwen, F. 2007, A&A, 474, 653

APPENDIX A: RECONSTRUCTION OF THE ECCENTRICITY DISTRIBUTION

The observed 2-dimensional distribution of (μ', γ) is binned on a grid with a step of 0.1 in μ' and 10° in γ, i.e. in the 15×9 array. The number of binaries in each grid cell is normalised by N, converting the result in the probability distribution.

The set of five basis functions is produced by simulating $N = 10^5$ binaries with eccentricities distributed uniformly in the intervals [0-0.2], [0.2-0.4], etc., including the sample selection criteria and measurement errors. The result is binned on the same 15×9 grid and normalised to make the sum over the grid equal one. These basis functions are shown in Figure A1.

Using these $k = 5$ simulated 2-dimensional distributions as basis functions, we can find the fractions of eccentricity in each bin f_k, $k = 1, 2, \ldots 5$ that match the real sample. The $15 \times 9 = 135$ grid cells are numbered sequentially by the index i, the values $b_i = n_i/N$ are fractions of the sample in each cell. Let $g_{i,k}$ be the basis functions derived by simulation. Then the problem is to find the 5-element vector $\mathbf{f}$ that minimises the difference

$$\sum_i \left(\sum_{k=1}^{5} g_{i,k} f_k - b_i \right)^2 + \alpha \sum_{k=1}^{5} f_k^2 = \min. \qquad \text{(A1)}$$

A regularisation term with a small parameter α is introduced in the left-hand side. Solution of the inverse problem amplifies the statistical noise. This can be improved by imposing additional condition that the distribution of eccentricity should be a smooth function, so we added its variance with a small coefficient α.

Equation A1 with additional constraint $\sum f_k = 1$ is solved by the standard method of Lagrange multipliers. The term $\lambda(\sum f_k - 1)$ is added to the left hand and partial derivatives over f_k and λ are equated to zero, leading to a linear system with 6 unknowns f_k, λ.

We increased α until it started to affect the residuals and found that $\alpha = 0.1$ is too large and tends to produce an almost uniform distribution, while $\alpha = 3\,10^{-3}$ is a good compromise. We used this value in the data processing and simulations.

Strictly speaking, Equation A1 should incorporate weights inversely proportional to the Poisson variance in each bin. However, for small numbers the Poisson distribution is asymmetric, whereas the least-squares method assumes normally distributed errors; this leads to a potential bias. A statistically rigorous treatment should maximize the likelihood function, but defining such a function using simulated samples is non-trivial. The histogram matching is a simpler practical alternative. Yet another reason why rigorous techniques do not always perform as expected is the mismatch between the assumptions (model) and the reality. In this study, the data can be affected to some extent by undetected subsystems. The unweighted least squares is relatively insensitive to a small number of deviant data points. We found that the residual difference between the real and fitted histograms is compatible with the Poisson statistics, meaning that the least-squares model adequately represents the data.

The restoration method was extensively tested on simulated samples with various $f(e)$. Table A1 compares the results of restoration using 20 independent simulated samples with $f(e) = 2e$ and $N = 475$ each. The average retrieved parameters f_k are close to their true values, while their rms scatter is similar to the errors estimated by bootstrap (compare to Table 5). When the weights proportional to $1/(1+n_i)$ are applied to mimic the Poisson statistics and to emphasize bins with small counts n_i, they introduce additional random noise and the scatter of the resulting f_k increases (see the last two lines of Table A1). Quasi-Poisson weights based on the modeled counts instead of the true n_i avoid the noise amplification, but the result might then become biased by the f_k priors used for the weight calculation.

Note that the parameters f_k are non-negative. We could use this additional constraint and apply the non-negative LS technique. However, the result would then be positively biased by random fluctuations. For this reason we prefer the linear LS. We also tried regularisation by singular value decomposition of the matrix, keeping the three largest singular values in its inversion; the α-regularization gives a lower noise.

Table A1. Test of the algorithm for $f(e) = 2e$

Case	f_1	f_2	f_3	f_4	f_5
True	0.04	0.12	0.24	0.28	0.36
No weight	0.03	0.13	0.21	0.28	0.36
	±0.02	0.05	0.06	0.05	0.04
Weighted	0.06	0.14	0.23	0.28	0.28
	±0.08	0.09	0.14	0.11	0.09

Instead of modelling the eccentricity distribution by 5 bins, we can describe it by a linear function $f(e) = 2f_{\rm lin}e + 1 - f_{\rm lin}$ or by a combination of thermal, uniform, and sine distributions (like a linear or quadratic polynomial). This alternative model requires only two or three basis functions and has one or two unknown parameters. It was also tested by simulations and fitted to the real data.

This paper has been typeset from a TEX/LATEX file prepared by the author.